Ingeniería Investigación y Tecnología
volumen XXVI (número 2), abril-junio 2025 1-7
ISSN 2594-0732 FI-UNAM artículo arbitrado
Información del artículo: Recibido: 17 de septiembre de 2024, aceptado: 3 de marzo de 2025

https://doi.org/10.22201/fi.25940732e.2025.26.2.012

Ingeniería
Investigación y
Tecnología

Effect of multipass welding on the microstructure of superduplex stainless steel

Efecto de la soldadura multipasos sobre la microestructura de un acero inoxidable superdúplex

Villalobos-Vera Doris Ivette (Corresponding author)
Tecnológico Nacional de México
Instituto Tecnológico de Veracruz
Welding and Foundry Laboratory
E-mail: doris.vv@veracruz.tecnm.mx
http://orcid.org/0000-0001-7365-1742

Mendoza-Bravo Ivan
Tecnológico Nacional de México
Instituto Tecnológico de Veracruz
Welding and Foundry Laboratory
E-mail: ivan.mb@veracruz.tecnm.mx
http://orcid.org/0000-0003-2907-7709

Valerio-Canales Gabriela
Tecnológico Nacional de México
Instituto Tecnológico de Veracruz
Department of Metal-Mechanics
E-mail: gabriela.vc@veracruz.tecnm.mx
https://orcid.org/0009-0004-1566-2194

Abstract

This work studies the influence of thermal cycles on the microstructure of a 2507 superduplex stainless steel (2507 SDSS) after being multipass-welded using the GMAW process with ER 2209 filler metal and two shielding gasses (Ar and Ar-6 %N). To calculate the thermal cycles experienced during welding, the heat flow equation for a thin plate was used. All samples were analyzed by optical microscopy and scanning electron microscopy to identify phases. The results showed particles of sigma phase in both the heat affected zone (HAZ) and welding metal (WM) in the ferrite/austenite grain boundary and intragranular, resulting in the loss of the microstructural balance of the superduplex stainless steel.
Keywords: Duplex stainless steel, microstructure, thermal cycles, GMAW, sigma phase.

Resumen

Este trabajo estudia la influencia de los ciclos térmicos sobre la microestructura del acero inoxidable superdúplex del tipo 2507 después de haber sido soldado mediante el proceso GMAW con el metal de aporte ER 2209 y dos tipos de gas de protección (Ar y Ar-6 %N). Para calcular los ciclos térmicos experimentados durante la soldadura multipasos, se utilizó la ecuación de flujo de calor para una placa delgada. Las muestras fueron analizadas mediante microscopía óptica y microscopía electrónica de barrido para identificar las fases. Los resultados mostraron partículas de fase sigma en la zona afectada térmicamente y en el metal de soldadura en los límites de grano ferrita/austenita y de forma intragranular, resultando en la pérdida del balance microestructural del acero inoxidable superdúplex.
Descriptores: Acero inoxidable superdúplex, microestructura, ciclos térmicos, GMAW, fase sigma.

https://doi.org/10.22201/fi.25940732e.2025.26.2.012

Introduction

Duplex stainless steels are used in highly corrosive environment such as in the petrochemical and offshore industries due to the high corrosion resistance and mechanical properties they offer (Zucato *et al*., 2002). They present equal amounts of ferrite (α) and austenite (γ), which confers a good combination of mechanical properties and corrosion resistance. These alloys have chromium, molybdenum, nickel and nitrogen as primary alloy elements and are often selected to fabricate components and complex parts using welding processes such as GMAW. As GMAW process is considered a high heat input process, the material undergoes thermal cycles that may promote the formation of secondary phases in the heat affected zone or even in the welding metal, disturbing the microstructural balance of ferrite/austenite. Several investigations have been developed to understand the formation of these secondary phases such as sigma phase (σ), nitrides, or carbides, which are known for reducing the mechanical properties and corrosion resistance; being the sigma phase the most detrimental (Chail, 2016). As all secondary phases are a function of time and temperature, the susceptibility to form sigma phase in zones of the welded joint because of the thermal cycles, increases when a multipass welding is performed.

If sigma phase forms in the heat affected zone or the welding metal, the balance of ferrite/austenite will be lost, and the final behavior will be altered. Several approaches have been made to calculate thermal cycles and cooling time using heat-flow equations based on the materials thickness (Easterling, 1992). Research made by Easterling (1992) and Sieurin & Sandström (2006) have showed a good estimation of thermal cycles and cooling time for duplex alloys.

Beside the welding process, it is also important to take into account the filler metal and shielding gas used, which are intended to keep the microstructural balance of ferrite/austenite in the welding metal (Başyiğit & Kurt, 2018). On the other hand, to anticipate if the filler metal is suitable to perform the welding, the WRC-1992 diagram is the most confident way to predict the final microstructure of ferrite/austenite in the welding of duplex alloys (Kotecki & Siewert, 1992) by the determination of the ferrite number although the WRC 1922 diagram does not consider thermal cycles. However, for duplex alloys, the determination of ferrite number remains important because sigma phase nucleates and grows from ferrite (Krishnan *et al.*, 1991). Since the percentage of ferrite is a concern for the final microstructure of welds, the ferrite number is considered to be approximately equivalent to the percentage of ferrite content (Hosseini *et al.*, 2019). Adding nitrogen to the shielding gas helps the formation of more austenite than ferrite, retarding in turn, the formation of ferrite and then the formation of sigma phase (Başyiğit & Kurt, 2018).

Sigma phase is formed mainly by chromium and molybdenum, the primary elements of ferrite, following the eutectoid transformation of $\alpha \rightarrow \gamma + \sigma$ (Magnabosco, 2009). That means that the amount of ferrite in the welding metal or the heat affected zone may transform into sigma phase as the amount of ferrite has been related to the amount of sigma phase (Magnabosco, 2009). Therefore, the main objective of this work is to study the influence of the multipass welding on the microstructural balance of ferrite/austenite in superduplex stainless steels.

Materials and methods

Plates of 2507 superduplex stainless steel with dimension of 30 cm x 8 cm x 0.6 cm were welded with GMAW process using ER 2209 filler metal and two shielding gases: Ar and Ar + 6 %N. The chemical composition of both materials is given in Table 1 according to the standard (ASTM, 2017). The Creq/Nieq ratio was calculated according to the WRC 1992 diagram (Kotecki & Siewert, 1992). The plates were prepared with a single V-bevel at a 45-degree angle with a root opening of 3 mm. The welds in Figure 1 required the deposition of three passes (root pass, filler pass and cover pass) to obtain full penetration and were deposited with an interpass temperature of ~850 °-900 °C which was measured using an Extech VIR50 dual laser infrared thermometer. This thermometer measures in the range of –50 °C to 2200 °C with an accuracy of ± 3.3 °C. The welding was performed perpendicular to the rolling direction. The heat input was calculated according to the welding parameters in Table 2 using formula q= AV/welding speed (Kou, 2003).

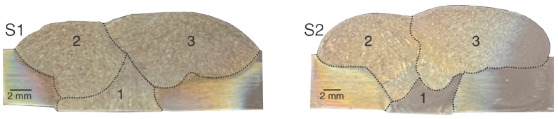

Figure 1. Macrographies of sample S1 and sample S2, showing full penetration and no defects

The thermal profile for specific points in the heat affected zone corresponding to the root pass was calculated according to the heat-flow equation (1) for a thin plate model (Easterling, 1992). The cooling time was also cal-

Table 1. Chemical composition of base and filler metal (wt %)

	C	Si	Mn	Ni	Cr	Mo	N	Cr_{eq}	Ni_{eq}	Cr_{eq}/Ni_{eq} ratio
2507 SDSS	0.03	0.40	.88	5.78	23.40	3.23	0.27	29.13	12.6	2.3
ER 2209	0.03	0.45	1.26	7.73	19.98	3.14	0.15	23.13	13.8	1.6

Table 2. Welding specifications

Sample ID	Base material	Filler metal	Shielding gas (20 L/min)	Current (A)	Voltage (V)	Welding speed (mm/min)	Heat input (kJ/mm)
S1	2507 SDSS	ER 2209	Ar	300	30	390	1.385
S2	2507 SDSS	ER 2209	Ar-6 %N	300	30	390	1.385

culated using equation (2) in the range of 1200 °C – 800 °C (Sieurin & Sandström, 2006), which is specifically for duplex stainless steel.

$$Tp - To = \left(\frac{2}{\pi e}\right)^{1/2}\left(\frac{q/v}{d\rho\varsigma 2r}\right) \quad (1)$$

$$\Delta t_{12/8} = \Delta t_{8/5}\frac{\frac{1}{1073-To}-\frac{1}{1473-To}}{\frac{1}{773-To}-\frac{1}{1073-To}}\Delta t = \frac{(q/v)^2}{4\pi\lambda\rho\varsigma\theta_2^2 d^2} \quad (2)$$

Where:

q = heat input
v = welding speed
d = thickness
ρ = specific heat
ς = density
r = distance from the heat source
T_0 = initial temperature (25 °C)

The distance from the heat source is 7 mm, which is the distance from the center of the bead to where the heat affected zone begins.

The estimation of ferrite number in the weld metal as well as the solidification mode was carried out by using the WRC-1992 diagram. This estimation was based on the chemical composition of the base material and the filler metal considering the Cr_{eq} and Ni_{eq} for each one.

The microstructural characterization was performed on the heat affected zone and the welding metal corresponding to the root pass. Standard techniques included grinding with SiC paper and polishing with 1 and 3 microns diamond paste. To reveal the microstructure all samples were electrochemically etched with KOH, which differentiates ferrite from austenite and sigma phase. The microstructure was characterized by OM and SEM coupled with EDS. The volumetric fraction of phases was calculated using an image analyzer.

Results and discussion

Microstructural analysis

Figure 2 shows the typical microstructure of the duplex alloy in the as-received condition consisting of ≈ 54 % ferrite and ≈ 46 % austenite. The grains are oriented to the rolling direction resulting in a balanced microstructure formed by islands of austenite embedded in a ferrite matrix with no secondary phases present. The KOH etching reveals the austenite phase in white color and ferrite phase in gray color. The EDS analysis of ferrite and austenite in Table 3 shows the high content of chromium and molybdenum in the ferrite compared to the austenite as expected.

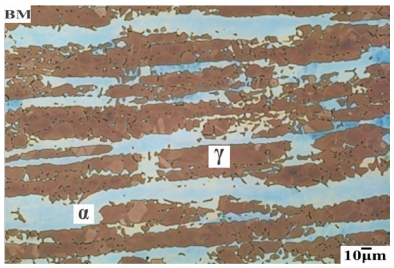

Figure 2. Microstructure of the as-received material 2507 SDSS

Table 3. EDS analysis of ferrite and austenite in the as-received condition 2507 SDSS

	Element Content (wt%)						
Phase	C	Cr	Ni	Mo	Mn	Si	Fe
γ	5.01	17.95	6.11	1.12	1.69	0.43	49.31
α	9.47	24.32	4.60	2.29	1.88	0.65	56.80

https://doi.org/10.22201/fi.25940732e.2025.26.2.012

Heat affected zone

Figure 3 and Figure 4 show the HAZ adjacent to the root pass composed by coarse-grained austenite and small particles of sigma phase within a ferritic matrix. The temperature and time in that zone were enough to allow the diffusional transformation from ferrite as the calculated time and temperature distribution in Figure 5 indicate that the HAZ stayed in the range of 1200 °C-800 °C for at least 2.86 s.

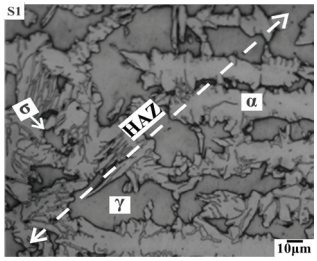

Figure 3. Heat affected zone in sample S1

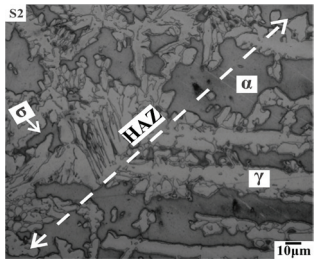

Figure 4. Heat affected zone in sample S2

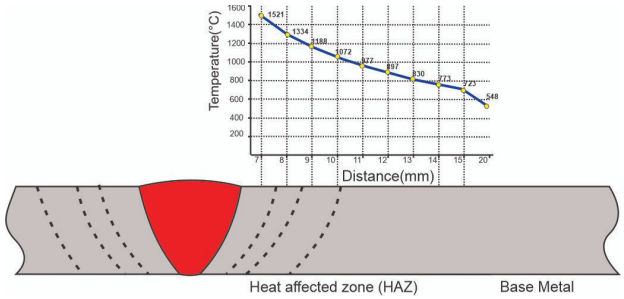

Figure 5. Heat distribution calculated for the root pass of the multipass welding

The cooling rate was about 130 °C/s, allowing the austenite to form along the ferrite grain boundaries at first, and then as Widmanstätten austenite or within the ferrite grains, having enough time to become coarser than the original grain (Lippold & Kotecki, 2005; Mohamed *et al*., 2017). The formation of sigma phase in the ferrite/austenite interface was permitted from ferrite grains since sigma is thermodynamically stable at temperatures above 800 °C. Compared to the base metal, the percentage of austenite increased in both samples (55 % for S1 and 52 % for S2). This microstructure indicates that this zone was considerable affected by the thermal cycles caused by the deposition of the filler pass and cover pass (Sadeghian *et al*., 2014).

Welding metal

The welding metals in Figure 6 and Figure 7 show three important features compared to the base metal: an austenite matrix, the presence of sigma phase and an insignificant amount of ferrite. According to the WRC 1992 diagram (Figure 8), the prediction of the resultant solidification mode is a mix of ferrite and austenite and the predicted ferrite number for the welding metal is FN = 27 approximately. However, it is evident that both welding metals lost the expected mix even though the filler metal is intended to keep the ferrite/austenite ratio at room temperature. This implies that the thermal cycles and cooling rate caused by the deposition of the passes play an important role on the final microstructure (Nowacki & Lukojć, 2005). Consequently, the decomposition of ferrite into sigma and austenite takes place at temperatures above 800 °C due to the deposition of the filler pass and cover pass. Compared to the base metal, the ferrite content decreased drastically while the austenite increased considerably in both samples: 15 %α – 73 %γ for S1 and 2 %α – 68 %γ for S2.

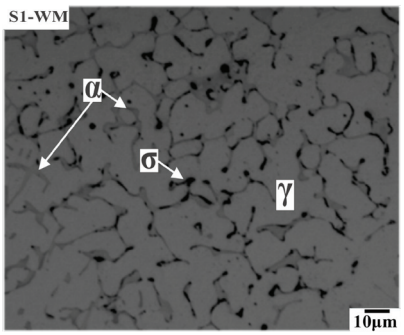

Figure 6. Microstructure of welding metal in sample S1

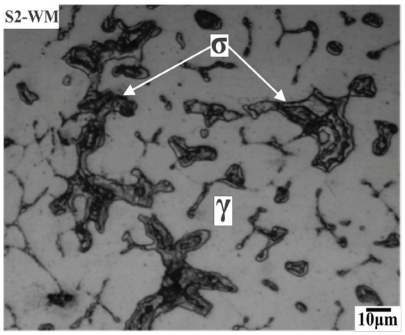

Figure 7. Microstructure of welding metal in sample S2

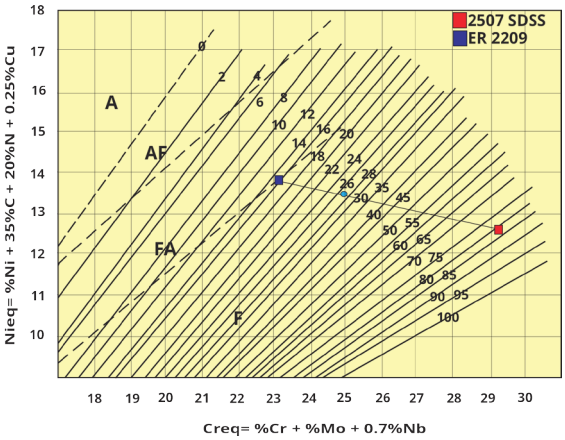

Figure 8. WRC-1992 diagram and calculated ferrite number based on the chemical composition of base metal and filler metal

The Creq/Nieq ratio denotes that the base material solidifies in a fully ferritic mode (Lippold & Kotecki, 2005) and hence, more ferrite than austenite at room temperature may be expected. However, the increment of austenite in both welding metals indicates that the thermal cycles experienced in that zone promoted a cooling rate slow enough to allow the nucleation and growth of austenite from ferrite in the solid state (Lippold and Kotecki, 2005). According to the calculated temperature distribution in Figure 5 for the heat affected zone, the welding metal corresponding to the root pass experienced at least temperatures in the range of 1200 °C-800 °C due to the deposition of the subsequent passes. Therefore, a slow cooling rate is promoted and the formation of austenite through a diffusion-driven process takes place. In addition to the use of the adequate filler metal to reach the ferrite/austenite balance in the welding metal, the heat input and the control of thermal cycles are important for a sound welding.

In Figure 6 particles of sigma phase are dispersed over the austenite matrix in the ferrite/austenite interface, nucleating in the grain boundary and growing through the center of the grain while in Figure 7 a blocky morphology of sigma phase with the absence of ferrite is observed. A closer examination of S1-WM in Figure 9 shows the occurrence of sigma phase inside the ferrite grain, presenting almost the total consumption of ferrite in some areas according to the eutectoid transformation of ferrite into sigma phase and secondary austenite. On the other hand, Figure 10 shows a drastic decomposition of ferrite into sigma phase in the middle of the grain and secondary austenite in S2-WM.

This transformation is the result of the diffusion of Cr and Mo from the ferrite itself (Padilha *et al*., 2012). If the diffusion occurs, the ferrite becomes thermodynamically unstable at temperatures around 800 °C where the sigma phase is stable, and therefore the formation of sigma phase and secondary austenite takes place. Based on the calculated time in Figure 5, the welding metal stayed at least 2.86 s in the temperature range of 1200 °C – 800 °C, leaving the material almost depleted or totally depleted of ferrite.

The amount of sigma phase in S1-WM is around 12 % and the presence of ferrite is limited by the amount of sigma phase. On the other hand, in S2-WM the total consumption of ferrite gives rise to a very high amount of sigma phase (30 %), depicting the eutectoid reaction of ferrite to secondary austenite and sigma. The addition of N through the shielding gas promoted the equilibrium of the austenite and therefore, the volume fraction of sigma phase is strongly related to the total ferrite consumption.

The microanalysis in Table 4 and Table 5 showed that sigma phase has the highest amount of Cr and Mo compared to austenite phase. Even though the filler

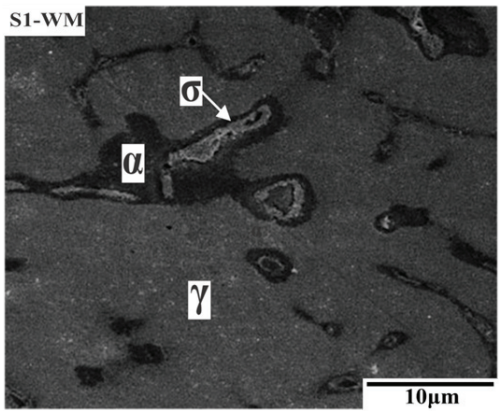

Figure 9. Microstructure of the welding metal for sample S1

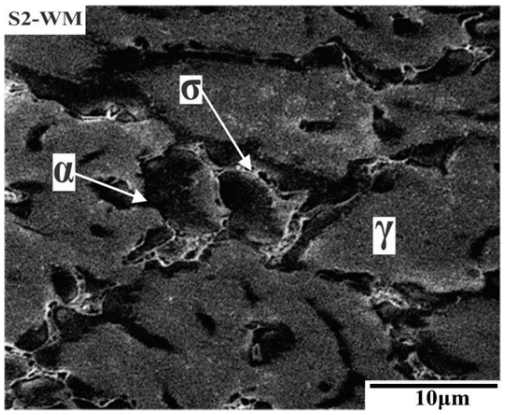

Figure 10. Microstructure of the welding metal for sample S2

Table 4. Microanalysis of ferrite, austenite and sigma phase in the welding metal of sample S1

	Element Content (wt%)						
Base material	C	Cr	Ni	Mo	Mn	Si	Fe
γ	5.01	17.95	6.11	1.12	1.69	0.43	49.31
δ	9.47	24.32	4.60	2.29	1.88	0.65	56.80
Welding metal							
γ	1.57	20.13	7.23	2.52	1.17	0.43	61.50
α	2.87	18.20	7.59	2.85	0.92	0.78	53.37
σ	1.57	21.60	5.15	4.18	0.93	0.65	59.36

Table 5. Microanalysis of ferrite, austenite and sigma phase in the welding metal of sample S2

	Element Content (wt%)						
Base material	C	Cr	Ni	Mo	Mn	Si	Fe
γ	5.01	17.95	6.11	1.12	1.69	0.43	49.31
α	9.47	24.32	4.60	2.29	1.88	0.65	56.80
Welding metal							
γ	1.21	18.19	7.27	2.39	0.42	0.69	64.25
α	2.66	16.43	7.86	2.44	0.40	1.09	56.49
σ	2.94	23.25	5.40	7.46	0.45	1.18	47.90

metals rich in Ni, Cr and N are intended to balance the final microstructure of the welding, the formation of sigma phase is inevitable.

Conclusions

Welding joints performed of super duplex stainless steels need to exhibit a balanced microstructure of ferrite and austenite at room temperature like the initial microstructure of the base metal to assure that the mechanical and metallurgical properties are maintained. For that reason, choosing a filler metal is of highly importance. In the case of the duplex alloys, the ER 2209 filler metal is suitable due to the amount of nickel and nitrogen, which promote the formation of austenite during the cooling from high temperatures, allowing the presence of austenite at room temperature and balancing the final microstructure of the weld along with the ferrite. If the austenite is not formed, high amounts of ferrite can be obtained in the welding metal. According to the thermal cycles experienced during welding, that portion of ferrite may transform to sigma phase following the eutectoid reaction transformation of ferrite into austenite and sigma phase.

On the other hand, the shielding gas may influence the final microstructure of the welding metal due to the addition of nitrogen. Therefore, it is also important to balance the amount of nitrogen since high amounts of nitrogen can be detrimental. The results showed that increasing the amount of nitrogen through the shielding gas, the final microstructure of the welding metal consists in austenite and sigma phase, indicating that the amount of ferrite diminished, allowing the nucleation of sigma phase at the ferrite/austenite interface, growing to the center of the grains, and eventually consuming all the ferrite grains.

Acknowledgements

The authors express their acknowledgement to Tecnológico Nacional de México for the financial support.

References

ASTM. (2017). A789/A789M-17. Standard Specification for Seamless and Welded Ferritic/Austenitic Stainless Steel Tubing for General Service.

Başyiğit, A., & Kurt, A. (2018). The effects of nitrogen gas on microstructural and mechanical properties of TIG welded S32205 duplex stainless steel. *Metals*, 8(4), 226. https://doi.org/10.3390/met8040226

Chail, C. K. (2016). Super and hyper duplex stainless steels: structures, properties and applications. *Procedia Structural Integrity*, 2, 1755-1762. https://doi.org/10.1016/j.prostr.2016.06.221

Easterling, K. (1992). *Introduction to the physical metallurgy of welding*. 2nd ed. Butterworth-Heinemann.

Hosseini, A., Hurtig, V., Eyzop, D., *et al.* (2019). Ferrite content measurement in super duplex stainless steel welds. *Weld World*, 63, 551-563. https://doi.org/10.1007/s40194-018-00681-1

Kotecki, D.J., & Siewert, T.A. (1992). WRC-1992 Constitution diagram for stainless steel weld metals: a modification of the WRC-1988 diagram. *Welding Journal*, 71.

Kou, S. (2003). *Welding Metallurgy*. 2nd ed. Wiley Interscience.

Krishnan, K. N., Prasad R. K., & Srinivas, V. (1991) Effect of initial ferrite content on phase transformations in niobium stabilized austenitic clad metals. *Journal of Materials Science*, 26, 407-411.

Lippold, J. C. & Kotecki, D. J. (2005). *Welding metallurgy and weldability of stainless steels.* Vol. 7. Wiley.

Magnabosco, R. (2009). Kinetics of sigma phase formation in a duplex stainless steel. *Materials Research*, 12 (3) 321-327. https://doi.org/10.1590/S1516-14392009000300012

Mohammed, G. R., Ishak, M., Aqida, S. N., & Abdulhadi, H. A. (2017). Effects of heat input on microstructure, corrosion and mechanical characteristics of welded austenitic and duplex stainless steels: A Review. *Metals*, 7(2), 39. https://doi.org/10.3390/met7020039

Nowacki, J., & Łukojć, A. (2005). Structure and properties of the heat-affected zone of duplex steels welded joints. *Journal of Materials Processing Technology*, 164, 1074-1081. https://doi.org/10.1016/j.jmatprotec.2005.02.243

Padilha, A., Tavares, C., & Martorano, M. (2012). Delta ferrite formation in austenitic stainless steel castings. *Materials Science Forum*, 733-738. http://dx.doi.org/10.4028/www.scientific.net/MSF.730-732.733

Sadeghian, M., Shamanian, M., & Shafyei, A. (2014). Effect of heat input on microstructure and mechanical properties of dissimilar joints between super duplex stainless steel and high strength low alloy steel. *Materials & Design*, 60, 678-684. https://doi.org/10.1016/j.matdes.2014.03.057

Sieurin, H., & Sandström, R. (2006). Austenite reformation in the heat-affected zone of duplex stainless steel 2205. *Materials Science and Engineering: A*, 418(1-2), 250-256. https://doi.org/10.1016/j.msea.2005.11.025

Zucato, I., Moreira, M. C., Machado, I. F., & Giampietri-Lebrão, S. M. (2002). Microstructural characterization and the effect of phase transformations on toughness of the UNS S31803 duplex stainless steel aged treated at 850 °C. *Materials Research*, 5(3), 385-389. https://doi.org/10.1590/S1516-14392002000300026

Cómo citar:

Villalobos-Vera, D. I., Mendoza-Bravo, I., & Valerio-Canales, G. (2025). Effect of multipass welding on the microstructure of superduplex stainless steel. *Ingeniería Investigación y Tecnología,* 26(02), 1-7. https://doi.org/10.22201/fi.25940732e.2025.26.2.012